

Onset of chaos in a single-phase power electronic inverter

Viktor Avrutin,^{1,2,a)} Erik Mosekilde,^{3,b)} Zhanybai T. Zhusubaliyev,^{4,c)} and Laura Gardini^{2,d)}

¹*Institute for Systems Theory and Automatic Control, University of Stuttgart, Pfaffenwaldring 9, 70550 Stuttgart, Germany*

²*Department of Economics, Society and Politics, University of Urbino, via Saffi 42, 61029 Urbino, Italy*

³*Department of Physics, The Technical University of Denmark, Fysikvej 309, 2800 Lyngby, Denmark*

⁴*Department of Computer Science, Southwest State University, 50 Years of October Str., 94, 305040 Kursk, Russia*

(Received 8 August 2014; accepted 3 April 2015; published online 24 April 2015)

Supported by experiments on a power electronic DC/AC converter, this paper considers an unusual transition from the domain of stable periodic dynamics (corresponding to the desired mode of operation) to chaotic dynamics. The behavior of the converter is studied by means of a 1D stroboscopic map derived from a non-autonomous ordinary differential equation with discontinuous right-hand side. By construction, this stroboscopic map has a high number of border points. It is shown that the onset of chaos occurs stepwise, via irregular cascades of different border collisions, some of which lead to bifurcations while others do not. © 2015 AIP Publishing LLC.

[<http://dx.doi.org/10.1063/1.4918299>]

Power electronic inverters (DC/AC converters) provide AC power from a DC source. Converters of this type play an important role in modern power engineering. They are used, for instance, as so-called grid-tie inverters to convert low voltage DC power from a solar panel into AC power. Other applications include their use as uninterruptible power supplies (UPS), active filters, flexible AC transmission systems (FACTS), voltage compensators, etc. The dynamics of such a system involves two external signals: a low frequency reference signal that defines the waveform of the desired output and a high frequency, pulse-modulated switching signal that, during each switching period, connects the load to the available DC supply voltage for a fraction of time that is controlled by the reference signal. From the view of nonlinear dynamics, power electronic converters are piecewise smooth dynamical systems and typically exhibit border-collision bifurcations. It is well-known that such bifurcations may lead to a direct transition from an attracting fixed point or cycle to chaos. The desired mode of operation for the inverter is an attracting cycle following the periodic reference cycle. However, as parameters are varied, small amplitude high frequency chaotic oscillations modulated by the low-frequency reference signal may appear. Remarkably, the boundaries in parameter space between domains of regular and chaotic dynamics form an unusually complex structure that appears not previously to have been described. We first illustrate how the regular and chaotic forms of dynamics arise in an experimental inverter system. Next, we transform the non-autonomous ordinary differential equation with discontinuous right hand side that describes the inverter into an autonomous, piecewise smooth 1D stroboscopic map for which the desired mode of operation of the inverter is an attracting

fixed point. By construction, this stroboscopic map displays a high number of border points, and under variation of the parameters, the dynamics of the map is essentially influenced by collisions with these border points. Some of the collisions lead to bifurcations that change the topological structure of state space. However, there are also collisions that do not affect the topological structure of state space. A stable fixed point, for instance, may cross a switching manifold and still remain stable. The high number of border points causes the collisions to occur in cascades such that a stable fixed point may undergo a number of border collisions without change of stability, or may be destabilized in a border collision bifurcation, to then be re-stabilized again in a border collision bifurcation at a slightly different parameter value. The irregular manner in which the border-collision bifurcations occur explains the unusual structure of the boundary between regular and chaotic domains.

I. INTRODUCTION

Electronic inverter systems play an important role in modern power engineering. Due to their ability to provide AC power from a DC source with high efficiency and by virtue of their relatively small size and low costs, converter systems of this type have found a broad range of applications in the private households as well as in the industry and transport sectors. At remote locations, where access to the power line is impossible, DC/AC converters can be used to power refrigerators, TV-sets, and other household appliances from the battery of a car.¹ Other applications include the use as so-called grid-tied inverters to convert low voltage DC power from solar panels into AC power at the line frequency and voltage.² Moreover, by providing an approach to connect high-voltage AC transmission lines without requiring precise frequency and phase synchronization, it is expected that

^{a)}Electronic mail: Avrutin.Viktor@ist.uni-stuttgart.de

^{b)}Electronic mail: Erik.Mosekilde@fysik.dtu.dk

^{c)}Electronic mail: Zhanybai@hotmail.com

^{d)}Electronic mail: Laura.Gardini@uniurb.it

inverter systems will make a significant contribution to the stabilization of the high-voltage power distribution system.³

The main ideas underlying the operation of power electronic inverters are (i) application of switching dynamics alternately connects the load to a positive and a negative version of the available DC supply voltage, (ii) the use of pulse-width modulation allows the fraction of time spent in each of the two configurations to be adjusted in accordance with the externally specified wave form, (iii) feedback regulation provides a simple approach to correct deviations from the desired mode, and (iv) operation at a relatively high switching frequency allows the ripple on the output voltage to be kept at acceptable levels with the use of relatively small filter components. At the same time, the feedback regulation introduces an additional source of interaction between the low-frequency power mode, the high-frequency switching cycle, and the endogenous dynamics of the filter circuit. This interaction gives birth to a variety of unusual nonlinear dynamic phenomena, including the newly reported phenomenon of phase synchronized quasiperiodicity⁴⁻⁶ and the irregular transition to deterministic chaos through a cascade of different border-collision bifurcations, reported in the present work.

Similar to other systems with switching control, power electronic converter systems can generally be modeled as piecewise smooth dynamical systems.⁷⁻⁹ Such systems are characterized by the fact that their phase space is divided into regions with different dynamics, separated from each other by so-called switching sets. In addition to the bifurcations occurring in smooth systems, piecewise smooth systems also show a variety of border-collision related phenomena which occur when an invariant set such as, for example, a cycle, collides with a switching set. When such a collision causes a change of the topological structure of the phase space of the system, it is called a border-collision bifurcation. An overview of border collision related phenomena may be found in the book by di Bernardo *et al.*,⁹ see also the recent publications by di Bernardo *et al.*,¹⁰ by Makarenko and Lamb,¹¹ and by Zhusubaliyev *et al.*¹²

In this paper, we consider a single-phase H-bridge inverter with a pulse-width modulated control. The behavior of such a DC/AC converter is represented by a non-autonomous ordinary differential equation with a discontinuous right-hand side. This equation leads us first to formulate a 1D non-autonomous piecewise-smooth map with two periodically modulated borders and, thereafter, to establish a 1D autonomous piecewise-smooth stroboscopic map. By its construction, this second map displays a high number of border points, and as one would expect, this structure leads to unusual sequences of bifurcations. The normal operational regime for the considered DC/AC converter is the regime of stable period-1 dynamics, corresponding to stable fixed points of the 1D autonomous stroboscopic map. As parameters are varied, this period-1 mode becomes unstable and the system shows oscillations in the form of a small-amplitude chaotic ripple that is modulated by the low-frequency external reference signal.

To illustrate these phenomena, Fig. 1 presents the experimentally observed wave forms for the output voltage of the single-phase H-bridge inverter. The system we consider in

the present paper is a variant of the inverter discussed by Zhusubaliyev *et al.*⁴ The difference between the two inverters regards the scheme of the output filter only. The single-phase pulse-width modulated H-bridge inverter considered in our previous work has an LC output filter, whereas the inverter considered in the present paper has a resistive-inductive load.¹ As a consequence, this inverter can be modeled by a 1D map discussed below, while a similarly obtained model of the inverter with LC filter considered in the cited work is 2D.

Fig. 1(a) shows the experimentally observed wave form of the output voltage for the regular period-1 dynamics under normal operational conditions. As one can see from the magnifications shown in Figs. 1(c) and 1(e), this wave form is characterized by the presence of high-frequency oscillations which in this case are quite regular. One can also observe how the amplitude of the ripple oscillations is modulated by the low frequency power mode such that the ripple nearly disappears when the instantaneous amplitude of the power mode is at its extrema. This is a direct consequence of the applied control scheme (see Fig. 2(b)).

Fig. 1(b) shows the experimentally observed wave form for the chaotic dynamics. As one can see, especially in the magnifications shown in Figs. 1(d) and 1(f), this wave form is characterized by the existence of quite irregular high-frequency oscillations that are modulated by the low-frequency external reference signal. Examples of the appearance of such small-amplitude chaotic ripple in the practical inverter systems can be found in the book by Kazmierkowski *et al.*¹

The purpose of the present work is to find explanations to the observed unusual phenomena. We show that the transition from a fixed point to chaos in the considered system is associated with the following phenomenon. For increasing values of a parameter (such as the feedback gain factor), the stable fixed point undergoes a sequence of border collisions. The first border collisions in such a sequence are associated with persistence of a stable fixed point (a fixed point crosses a border moving from one branch of the map to the next one without changing its stability). As the value of the parameter is further increased, we observe that, at some border collision, the fixed point becomes unstable, and a different attractor (a cycle or a chaotic attractor) appears. However, this destabilization of the fixed point is not ultimate as, at one of the next border collisions, the fixed point may become stable again. Such a temporary destabilization with a subsequent restabilization of the fixed point occurs more and more frequently, the intervals of stability of the fixed point shrink, and after some transition (destabilization), the fixed point is not restabilized again. This route to chaos via an irregular sequence of border collisions differs essentially from other routes to chaos (such as a regular period-doubling cascade typical for smooth maps and a direct transition from a stable fixed point to chaos typical for piecewise-smooth maps). To our knowledge, this type of phenomenon, leading to an unusual and fairly complicated form of the boundary between the regions of stability of fixed points and the region associated with chaotic dynamics, has not previously been reported.

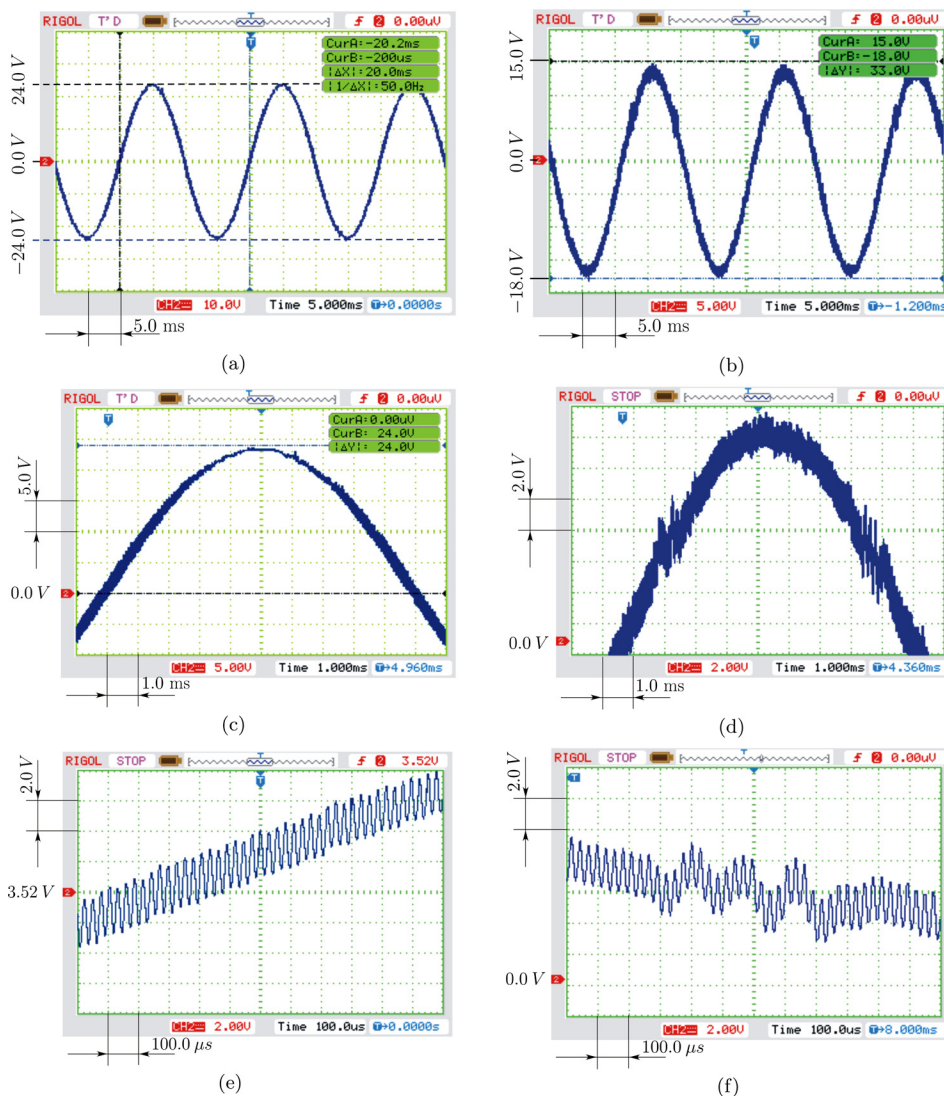


FIG. 1. Examples of the output signals of an inverter (a) in the regime of a stable period-1 dynamics and (b) in the chaotic regime, as observed experimentally on the screen of a digital oscilloscope. (c) and (e) Magnified parts of the wave form in (a), and (d) and (f) of the wave form in (b). The experimental setup is similar to that described by Zhusubaliyev *et al.*⁴ Note that the high-frequency ripple oscillations are most pronounced during the up-and downswing phases of the low-frequency power mode. This is also the phases where the chaotic variations first become noticeable.

In the present work, we discuss only the first steps towards understanding of the observed phenomena. Therefore, the aims of the present paper do not include any rigorous proofs or generalizations. After introduction of the considered model (which can be seen, however, as representative for a broad class of DC/AC converters), the transition to chaos mentioned above is studied using heuristic considerations based on results obtained numerically. At the present stage, no analytical theorems can be provided, so that we restrict ourselves to describing the phenomenon and leave its more rigorous treatment for future work.

The paper is organized as follows. In Sec. II, we describe the considered inverter (Sec. II A), its model given by a non-autonomous ordinary differential equation with a discontinuous right-hand side (Sec. II B), the corresponding 1D non-autonomous piecewise-smooth map and the resulting 1D autonomous piecewise-smooth stroboscopic map (Sec. II C). In Sec. III, we discuss the bifurcation phenomena occurring in the considered system and explain the mechanisms leading from stable fixed points to chaotic dynamics via cascades of border collisions. The obtained results are summarized in Sec. IV.

II. DESCRIPTION OF THE SYSTEM

A. Pulse-width modulated single-phase inverter

Figure 2(a) shows a schematic diagram of the pulse-width modulated (PWM) H-bridge, single-phase inverter to be considered in this paper, and Fig. 2(b) illustrates the generation of the control signal used to operate the four switches S_1 – S_4 that play an essential role in the functioning of the inverter.

The switches are operated by the sinusoidal pulse-width modulator. This implies that a feedback signal proportional to the AC output signal is compared with a reference sinusoidal voltage $V_{\text{ref}}(t) = V_m \cdot \cos(2\pi t/ma)$ of frequency $f_{\text{ref}} = 1/T$, $T = ma$, and amplitude V_m to generate the control voltage $V_{\text{con}}(t)$ (modulating signal). Here, a denotes the ramp period (the period of the clock signal V_{clock}) and m is referred to as the frequency modulation ratio, i.e., the number of clock cycles during the period T of the reference signal. The frequency modulation ratio obviously plays an important role in determining the accuracy with which the reference signal can be reproduced by the output current.

In the circuit diagram Fig. 2(a), E_0 represents the available DC-source voltage and $i(t)$ is the AC-current supplied to

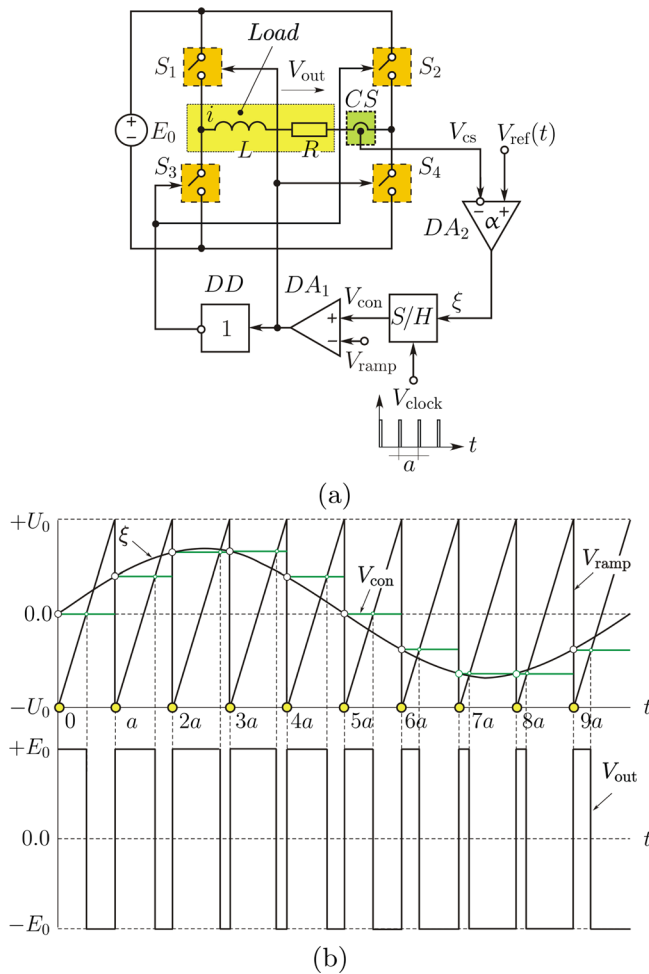


FIG. 2. (a) Schematic diagram of the considered PWM H-bridge single-phase inverter. E_0 is the externally supplied DC-voltage, and i is the AC-current supplied to the RL (resistive-inductive) load. CS is the current sensor, $V_{\text{ref}}(t) = V_m \cdot \cos(2\pi t/ma)$ the sinusoidal reference voltage, $V_{\text{cs}}(t) = \beta i(t)$ is the output voltage of the current sensor, and $\xi(t) = \alpha(V_{\text{ref}}(t) - \beta i(t))$ the error signal. (b) Sketch of the current-mode control applied to generate the switching signals. The sample-and-hold unit S/H detects the error signal $\xi(t)$ at the beginning of each clock time. This produces the control signal $V_{\text{con}}(t)$ that together with the ramp function $V_{\text{ramp}}(t)$ generates the switching signal to the switches S_1 , S_4 , and S_2 , S_3 . The four switches operate in pairs such that S_1 and S_4 are on while S_2 and S_3 are off, and *vice versa*. As long as $V_{\text{con}}(t) > V_{\text{ramp}}(t)$, switches S_1 , S_4 are on and S_2 , S_3 are off, while S_1 , S_4 are off and S_2 , S_3 on for $V_{\text{con}}(t) < V_{\text{ramp}}(t)$.

the load. R and L represent the resistive and inductive components of the load, and CS is the current sensor. The control signal $V_{\text{con}}(t)$ is compared with a sawtooth wave form $V_{\text{ramp}}(t)$ to generate the switching signal. The four switches of the bridge structure operate in pairs such that S_1 and S_4 are closed when S_2 and S_3 are open, and *vice versa*. When S_1 , S_4 are on and S_2 , S_3 are off, a positive voltage E_0 will be applied to the load; and when S_1 , S_4 are off and S_2 , S_3 are on, this voltage is reversed. The switches S_1 , S_4 are turned on and S_2 , S_3 are turned off at the beginning of every ramp period a . When the ramp voltage exceeds the value of the control voltage $V_{\text{con}}(t)$ during the ramp cycle, then the switches S_1 , S_4 are turned off and S_2 , S_3 are turned on (this is sometimes called a pulse-width modulation of the first kind).

In order to generate the switching signal to the inverter, the corrector amplifier DA_2 first determines the error signal

$\xi(t) = \alpha(V_{\text{ref}}(t) - \beta i(t))$ that measures the difference between the reference voltage $V_{\text{ref}}(t)$ and output voltage $V_{\text{cs}}(t) = \beta i(t)$ of the current sensor. Here, α is the corrector gain factor and β is referred to as the current sensor sensitivity parameter. As illustrated in Fig. 2(b), the sample-and-hold unit S/H reads the error signal $\xi(t)$ at every clock time $t = ka$, $k = 0, 1, 2, \dots$ and maintains it for the following switching period. This produces the control signal $V_{\text{con}}(t)$. Finally, the comparator DA_1 compares this control signal from the sample-and-hold unit with a periodic ramp function $V_{\text{ramp}}(t)$ in order to generate the switching signals to the switches S_1 , S_4 , and S_2 , S_3 . The ramp function $V_{\text{ramp}}(t)$ varies from $-U_0$ to $+U_0$ and in synchrony with the clock signal. If $V_{\text{con}}(t) \geq +U_0$ or $V_{\text{con}}(t) \leq -U_0$ the modulator is saturated. In the first case, i.e., if $V_{\text{con}}(t) \geq +U_0$, the duration of the positive pulse (see Fig. 2(b)) is equal to the ramp period a , and in the second case (i.e., if $V_{\text{con}}(t) \leq -U_0$) it is equal to zero.

The normal operational regime for the considered inverter, i.e., the regime of stable periodic dynamics with the period $T = ma$, is illustrated in Figs. 3(a) and 3(b). In this figure, showing the numerically calculated wave form for the load current $i(t)$, one can clearly identify the oscillations related to the low-frequency sinusoidal reference signal and the superimposed rapid modulations associated with the high-frequency switching cycle. This is similar to the experimental results presented in Fig. 1(a). When attempting to obtain a faster and more accurate control of the inverter output signal by increasing the corrector gain factor α , the periodic dynamics corresponding to the normal operational regime may become unstable and chaotic oscillations may appear. As illustrated in Figs. 3(c) and 3(d), in this case the large scale dynamics essentially maintains the characteristics of a regular cycle defined by the reference signal, but, similar to the experimental results shown in Fig. 1(b), the rapid modulations associated with the switching process are chaotic.

B. Continuous-time model

The dynamics of a single-phase PWM H-bridge inverter described above may be represented by the following non-autonomous differential equation with a discontinuous right hand side:

$$L \frac{di}{dt} = -Ri + E_0 K_F(t). \quad (1)$$

Here, the switching function

$$\begin{aligned} K_F(t) &= \text{sign}(V_{\text{con}}(t) - V_{\text{ramp}}(t)), \\ \text{with } V_{\text{ramp}}(t) &= U_0 \left(t/a - [t/a] - \frac{1}{2} \right), \\ V_{\text{con}}(t) &= \xi(t)|_{t=a[t/a]}, \\ \xi(t) &= \alpha(V_{\text{ref}}(t) - \beta i(t)), \\ V_{\text{ref}}(t) &= V_m \cos\left(\frac{2\pi t}{ma}\right) \end{aligned} \quad (2)$$

describes the operation of the four switches S_1 , S_2 , S_3 , and S_4 . The number $[t/a]$ is the largest integer number not greater than t/a (i.e., the integer part, or floor, of t/a).

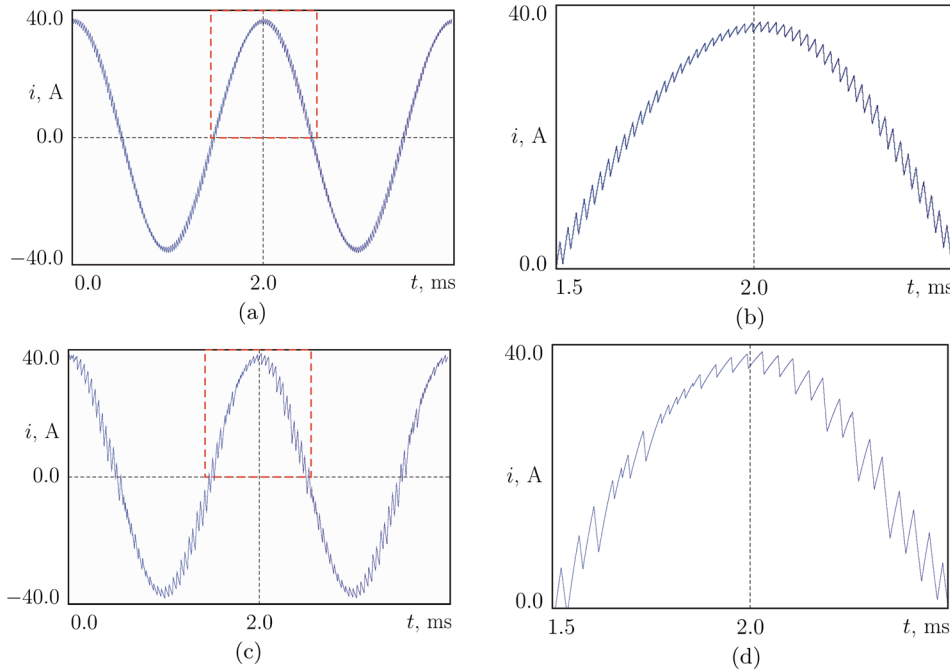


FIG. 3. (a) Numerically observed wave forms for the load current i of the single-phase PWM H-bridge inverter under regular period-1 operation with $\alpha = 4.0$, $m = 100$. Note the rapid fluctuations stemming from the finite frequency modulation ratio. (b) Magnified part of the temporal variation (a) as outlined by the red rectangle. (c) Wave form observed after the transition to an unusual form of chaotic dynamics for $\alpha = 6.0$. (d) Magnified part of the temporal variation (c) that is outlined by the red rectangle. The transition to chaos mainly affects the ripple associated with the switching dynamics.

Let us introduce the dimensionless dynamic variable $x = \frac{Ri}{E_0}$, the dimensionless time variable $\bar{t} = \frac{t}{a}$, and the following set of dimensionless parameters:

$$P = \frac{R}{\beta E_*} U_0; \quad q = \frac{R}{\beta E_*} V_m; \quad \Gamma = \frac{E_0}{E_*}; \quad \lambda = -\frac{R}{L} a.$$

The parameter P controls the amplitude of the ramp function, q represents the amplitude of the reference voltage, and Γ represents the DC source voltage, all normalized with respect to $E_* = 1 \text{ V}$. The absolute value of λ is proportional to the reciprocal of the time constant of the converter filter, normalized with respect to the period a of the ramp signal. In these terms, Eq. (1) can be rewritten in the form

$$\dot{x} = \begin{cases} g_+(x) = \lambda(x - 1), & \text{if } \zeta(\bar{t}, x) > 0, \\ g_-(x) = \lambda(x + 1), & \text{if } \zeta(\bar{t}, x) < 0, \end{cases} \quad (3)$$

where \dot{x} denotes the derivative of x with respect to \bar{t} . The scalar function $\zeta(\bar{t}, x)$ determines the switching manifold

$$\Sigma = \{(\bar{t}, x) : \zeta(\bar{t}, x) = 0\}, \quad \zeta(\bar{t}, x) = \varphi(\bar{t}, x) - \eta(\bar{t})$$

that separates the state space into two different regions

$$\Sigma_+ = \{(\bar{t}, x) : \zeta(\bar{t}, x) > 0\}, \quad \Sigma_- = \{(\bar{t}, x) : \zeta(\bar{t}, x) < 0\},$$

with

$$\varphi(\bar{t}, x) = \frac{q}{\Gamma} \cos\left(\frac{2\pi[\bar{t}]}{m}\right) - x(\bar{t})|_{\bar{t}=[\bar{t}]};$$

$$\eta(\bar{t}) = \frac{2P}{\alpha\Gamma} \left(\bar{t} - [\bar{t}] - \frac{1}{2}\right), \quad [\bar{t}] = k, \quad k = 0, 1, 2, \dots$$

The function $\varphi(\bar{t})$ represents the normalized control signal $V_{\text{con}}(t)$, i.e., the output signal from the sample-and-hold unit. The sawtooth function $\eta(\bar{t})$ is a periodically repeated ramp function with the ramp period 1, i.e., $\eta(\bar{t} + 1) \equiv \eta(\bar{t})$. The value $[\bar{t}] = k$, $k = 0, 1, 2, \dots$ is the normalized discrete time variable.

Note that the function $\zeta(\bar{t}, x)$ has a nonvanishing gradient $\nabla\zeta = (\partial\zeta/\partial\bar{t}, \partial\zeta/\partial x)$ on Σ . For points $(\bar{t}, x) \in \Sigma$ of the switching manifold we have

$$\langle \nabla\zeta, (1, g_+) \rangle \cdot \langle \nabla\zeta, (1, g_-) \rangle > 0$$

by virtue of the fact that

$$\langle \nabla\zeta, (1, g_{\pm}) \rangle = \frac{\partial\zeta(\bar{t}, x)}{\partial\bar{t}} + \frac{\partial\zeta(\bar{t}, x)}{\partial x} g_{\pm}(x) = -\frac{2P}{\alpha\Gamma} < 0.$$

Here $\langle \cdot, \cdot \rangle$ denotes the standard scalar product. This result implies that any solution of Eq. (3) with an initial condition in Σ_+ which hits after some time the switching manifold Σ , crosses it transversally and proceeds into the region Σ_- .

In the following simulations, we shall use $R = 1.0 \Omega$, $L = 10^{-4} \text{ H}$, $V_m = 4.0 \text{ V}$, $U_0 = 2.0 \text{ V}$, $a = 2 \cdot 10^{-5} \text{ s}$, $\beta = 0.1 \Omega$, and $m = 100$. These values are chosen in accordance with the parameters of the experimental setup. For the normalized system, this implies that $P = 20.0$, $q = 40.0$, and $\lambda = -0.2$. The corrector gain factor α and the normalized input voltage Γ are used as control parameters: $\alpha > 0$, $25.0 < \Gamma < 60.0$. It is not easy in practice to decide on the optimal structure of the feedback corrector, its parameters and the kind of pulse-width modulation to be used in order to attain the desired dynamical characteristics of the operating mode. Moreover, under realistic conditions both the available DC voltage and the load

resistance are likely to vary over time. The choice of the above pair of varied parameters is motivated by the wish to involve one parameter (such as the corrector gain factor α) that represents the control structure of the system and one parameter (such as the available DC voltage Γ) that represents the external conditions of operation. We emphasize, however, that preliminary experiments with other parameter combinations have shown results similar to those that we present here.

C. Piecewise-smooth map

By direct integration of the equations of motion for the continuous-time system (3) ramp period by ramp period, our investigation is reduced to the analysis of the piecewise-smooth map:

$$x_{k+1} = F(x_k, k), \quad k = 0, 1, 2, \dots \tag{4}$$

with

$$F(x_k, k) = \begin{cases} F_{\mathcal{L}}(x_k) = e^{\lambda}(x_k - 1) + 1, & \text{if } x_k \leq s_k^-; \\ F_{\mathcal{M}}(x_k) = e^{\lambda}(x_k - 1) + 2e^{\lambda(1-z_k)} - 1, & \text{if } s_k^- < x_k < s_k^+; \\ F_{\mathcal{R}}(x_k) = e^{\lambda}(x_k + 1) - 1, & \text{if } x_k \geq s_k^+; \end{cases} \tag{5a}$$

$$s_k^+ = \frac{q}{\Gamma} \cos\left(\frac{2\pi k}{m}\right) + \frac{P}{\alpha\Gamma}, \quad s_k^- = \frac{q}{\Gamma} \cos\left(\frac{2\pi k}{m}\right) - \frac{P}{\alpha\Gamma}, \tag{5b}$$

$$z_k = \alpha \cos\left(\frac{2\pi k}{m}\right) - \frac{\alpha\Gamma}{2P} x_k + \frac{1}{2}, \quad 0 \leq z_k \leq 1.0. \tag{5c}$$

If $x_k \geq s_k^+$ or $x_k \leq s_k^-$ the modulator is saturated. The pulse duration z_k is then equal to 1 (i.e., equal to the period of the ramp function $\eta(\bar{t})$) if $x_k \leq s_k^-$ and equal to zero if $x_k \geq s_k^+$.

The map (4) is a non-autonomous 1D map that can easily be transformed into a 2D autonomous map. Moreover, as the cosine function in Eq. (5) is m -periodic, for any x the equality

$$F(x, k) = F(x, k + m) \tag{6}$$

is satisfied. Therefore, the m th iterate

$$\begin{aligned} x_{k+1} &= f^m(x_k) \\ &= F(F(\dots F(F(x_k, 0), 1)\dots), m-2), m-1) \end{aligned} \tag{7}$$

represents a 1D stroboscopic map for the 2D autonomous variant of map (4) and completely reflects the dynamics of that map.

To understand the properties of map (7), it is worth noticing that for each fixed $k \in \{0, \dots, m-1\}$ the function $F(x, k)$ is a continuous piecewise-smooth bimodal function. On the two outer partitions (i.e., for $x_k \leq s_k^-$ and for $x_k \geq s_k^+$), the function F is defined by linearly increasing branches $F_{\mathcal{L}}$ and $F_{\mathcal{R}}$, whereas on the middle partition, i.e., for $s_k^- < x_k < s_k^+$, it has a non-linear decreasing branch $F_{\mathcal{M}}$. The shape of the function $F(x, k)$ is illustrated in Fig. 4(a) which shows the functions $F(x, 0)$ and $F(x, 7)$. As one can see, what changes when varying k are the border points s_k^-, s_k^+ and the middle non-linear branch $F_{\mathcal{M}}$, whereas the outer linear branches $F_{\mathcal{L}}, F_{\mathcal{R}}$ remain the same for all k .

An example of the shape of the function f^m for $m = 100$ is shown in Figs. 4(b)–4(d). Clearly, it is a continuous 1D piecewise-smooth map. However, depending on other

parameters, the number of border points of this map may grow exponentially when increasing m . These border points are given by $s_k^{\pm}, k = 0, \dots, m-1$ of F and their preimages. As for each k , the points s_k^{\pm} are points of local extrema of F , each border point of f^m is a point of a local extremum for this map.

Note that the stable period-1 dynamics with $\bar{T} = m$ of the continuous-time system (3) which corresponds to the normal operational regime of the considered class of converter systems is represented in the map (7) by a stable fixed point. Accordingly, our goal is reduced now to the investigation of the stability domains of the fixed points of map (7), and in particular, of its boundary.

III. BOUNDARY OF THE STABILITY DOMAIN OF FIXED POINTS

Figure 5(a) provides an overview of an interesting part of the bifurcation structure that can be observed in the (α, Γ) -parameter plane for the map (7). Recall that α is the corrector gain factor and Γ is the normalized DC supply voltage. In the left part of this diagram, where the corrector gain factor is relatively small, we observe the region Π_1 of stability of a unique fixed point. This fixed point represents the intended mode of operation for the inverter. The white region Π_{∞} observed for higher values of the corrector gain factor, and particularly pronounced, for relative high values of the DC supply voltage represents a region of chaotic dynamics. It is interesting to see how the transition between these two regions takes an unusual and fairly complicated form.

In the upper left corner of the bifurcation diagram shown in Fig. 5(a), we observe the region $\Pi_{1,1}$ where two stable fixed points coexist. The transition from Π_1 to $\Pi_{1,1}$ involves the destabilization of the original fixed point and the birth of a pair of new stable fixed points along the pitchfork bifurcation curve N_p . This process is illustrated in Fig. 6(a) that shows the variation of the normalized output current x as a function of the corrector gain factor. At the point α_p (corresponding to the curve N_p in Fig. 5(a)), the eigenvalue ρ of

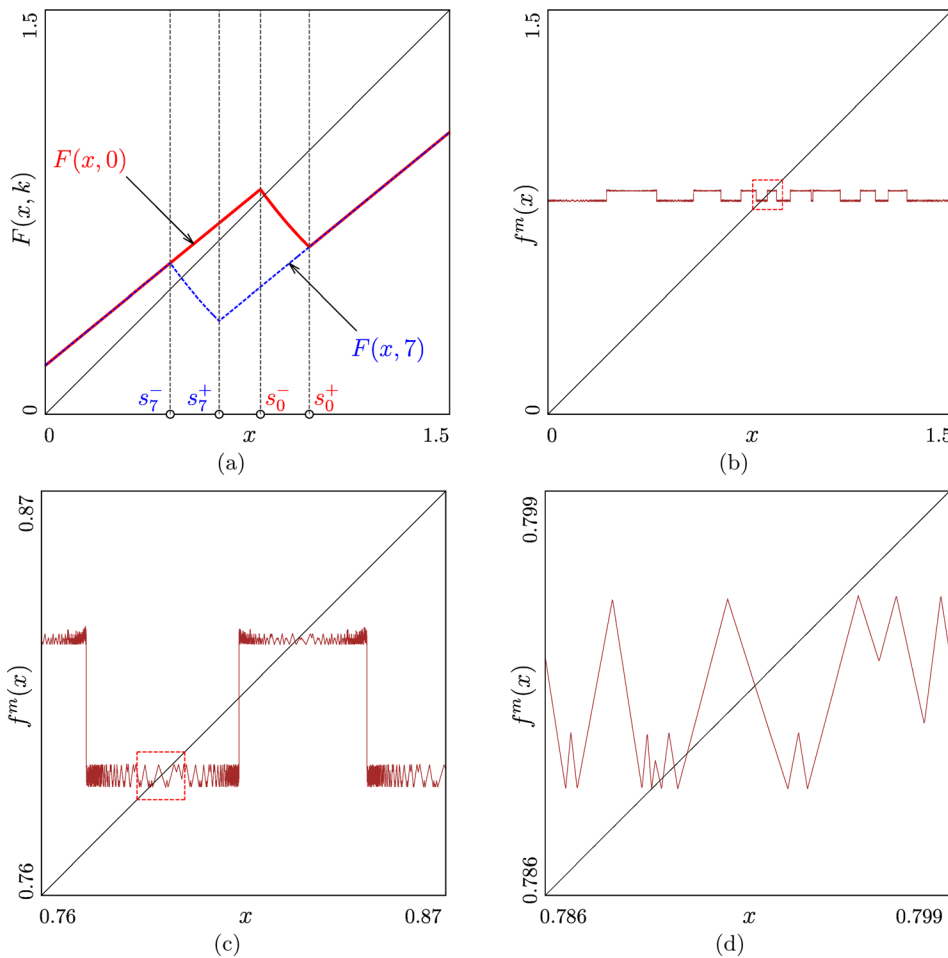


FIG. 4. (a) Function $F(x, k)$ defined by Eq. (5) at $k=0$ and at $k=7$. (b) Function f^m defined by Eq. (7). (c) and (d) Magnifications of the red rectangles outlined in (b) and (c), respectively. Parameters: $\alpha=4.9, \Gamma=45, m=100$.

the fixed point crosses through $+1$ (see Fig. 6(b)). The loss of stability for the fixed point leads to the appearance of two new stable fixed points.

The most striking feature of Fig. 5 is the unusual form of the transition between the stability domain of fixed points $\Pi_1 \cup \Pi_{1,1}$ and the chaotic domain Π_∞ . The sequence of magnifications as shown in Figs. 5(b)–5(d) indicates a fine structure of rhomboid regions related to fixed points which may be surrounded by regions corresponding to 2- and 4-cycles (marked in Fig. 5(d) with Π_2 and Π_4 , respectively) and partially overlapping with Π_∞ (see regions marked with $\Pi_{1,\infty}$ in Fig. 5(d) in which a stable fixed point and a chaotic attractor coexist). Although the sequence of periods (1, 2, 4) resembles the beginning of a period-doubling cascade, the shape of the associated regions is inconsistent with such cascades. In fact, some of the regions associated with a stable fixed point are surrounded by regions associated with a stable 2-cycle, while others are not. Similarly, a few of 2-cycles are followed by 4-cycles, while most of them are not, and not a single 8-cycle was detected. The above description raises a number of questions about the nature of the mechanisms responsible for the formation of such a frayed transition zone as observed between $\Pi_1 \cup \Pi_{1,1}$ and Π_∞ . One such question concerns the possibility of describing the transition analytically.¹³ A fixed point x_p can be found as a solution of the equation

$$x_p = F(\dots F(F(x_p, p), 1) \dots), p + m - 1), \quad p = k, \dots, m - 1 + k, \quad k = 0, \dots, m - 1. \quad (8)$$

The stability of the fixed point is determined by the condition $|\rho| < 1$ where

$$\rho = \prod_{p=0}^{m-1} \left. \frac{\partial F(x, p)}{\partial x} \right|_{x=x_p} \quad (9)$$

and

$$\frac{\partial F(x, p)}{\partial x} = \begin{cases} \frac{\partial F_{\mathcal{M}}(x)}{\partial x} = e^\lambda + \frac{\lambda \alpha \Gamma}{P} e^{\lambda(1-z_p)} & \text{if } s_p^- < x < s_p^+; \\ \frac{\partial F_{\mathcal{L}}(x)}{\partial x} = \frac{\partial F_{\mathcal{R}}(x)}{\partial x} = e^\lambda & \text{otherwise} \end{cases}$$

and the values s_p^\pm, z_p are given by Eqs. (5b) and (5c). However, Eq. (8) can be solved only numerically. Moreover, it is unclear for which particular sequence of applications of functions $F_{\mathcal{L}}, F_{\mathcal{M}}$, and $F_{\mathcal{R}}$ that Eq. (8) must be solved in order to detect the boundary between regular and chaotic domains. Therefore, the results presented below are obtained numerically. Stable sets are found by forward iterations of map (7). Coexisting attractors are detected by using an appropriate number of different initial values. Unstable

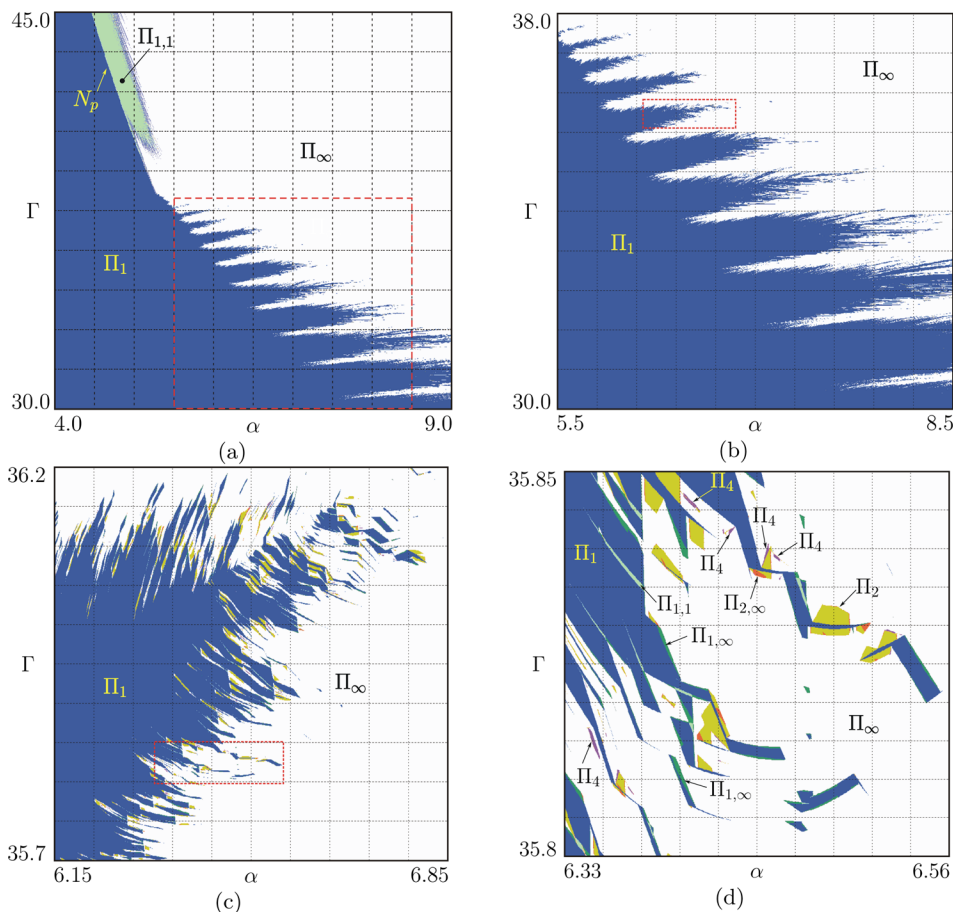


FIG. 5. Bifurcation structure of the parameter plane (α, Γ) . (a) Overview of the mode distribution. (b)–(d) Subsequent magnifications of the lower right part of (a). Π_1 is the domain of stability for a single fixed point, and $\Pi_{1,1}$ is the domain where two stable fixed points coexist. Π_2 and Π_4 are domains of stability for 2- and 4-cycles, respectively. $\Pi_{1,\infty}$ and $\Pi_{2,\infty}$ are the regions of coexistence of a stable fixed point and of a 2-cycle with a chaotic attractor, respectively, and Π_∞ is the region of chaotic dynamics. N_p is the pitchfork bifurcation curve.

cycles are detected by the variant of the cell-to-cell mapping method^{14,15} described in Ref. 16. Multiplier ρ of the fixed point is calculated by Eq. (9).

When investigating the boundary of the stability domain for fixed points of the map (7), it is natural to start by asking what types of bifurcations such fixed points may undergo. In addition to smooth bifurcations (as, for example, the pitchfork bifurcation discussed above) the fixed points may undergo different forms of border-collision bifurcations. In general (apart from codimension-two bifurcation cases), to predict the dynamics after such a bifurcation, the one-dimensional continuous piecewise linear map with one border point, known as the skew tent map, can be used as a normal form. The bifurcation structure of the skew tent map has been completely described (see, e.g., the papers 17–20). Then, for a general piecewise smooth continuous map $x_{n+1} = g(x_n)$ the behavior after a border collision of a fixed point can be obtained from the behavior of the skew tent map with the slopes given by the left- and right-side derivatives of g evaluated at the fixed point at the moment of the bifurcation. In principle, it is possible to evaluate numerically these derivatives for map (7), thus predicting the behavior after the bifurcation. However, this approach only provides a description of a single border-collision bifurcation and not of the overall frayed transition zone between periodic and chaotic domains which is evidently formed by a high number of such bifurcations following each other in a quite irregular manner (see Figs. 5(c) and 5(d)). Therefore, for the purposes of the present paper we restrict the analysis

to numerical experiments. In particular, we shall discuss the following phenomena:

- (a) Border collisions associated with persistence of a stable fixed point. Indeed, if both the left-side and the right-side derivative of f^m at the border point does not exceed one in modulus, then after the border collision there is a stable fixed point located on the next branch of f^m . Clearly, these border collisions occur not at the boundary of the stability domain of fixed points, but inside this domain.
- (b) Border-collision period-doubling bifurcations leading to the appearance of a stable 2-cycle.
- (c) Transitions from a stable fixed point to an n -band chaotic attractor with $n = 2^\ell, \ell = 0, 1, 2, \dots$

An example of a sequence of border collisions associated with persistence of stable fixed points (case (a) mentioned above) is shown in Fig. 7. This may occur both for the two fixed points existing after the pitchfork bifurcation (see Fig. 7(a)), and for other parameter values when the pitchfork bifurcation does not occur (see Fig. 7(b)). The mechanism leading to the appearance of such cascades is illustrated in Fig. 7(c). As one can see, for increasing values of α a stable fixed point of map (7), while remaining stable, moves from one branch of f^m to the next. Note that the dependence of the values of f^m on α is non-monotonous, so that when α increases the values of f^m may increase or decrease, as illustrated in Fig. 7(c). Therefore, several border collisions of a fixed point with the same border point of f^m are possible.

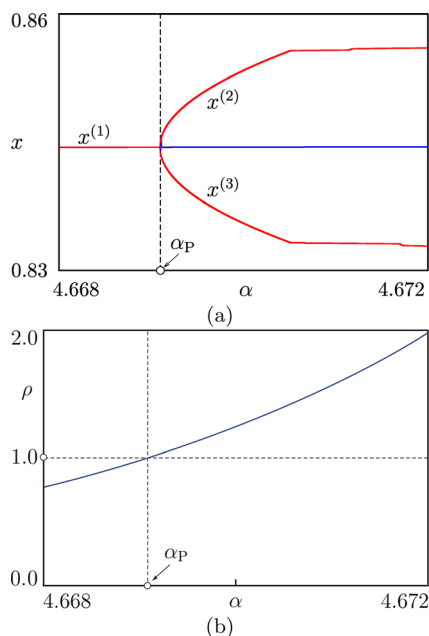


FIG. 6. (a) Pitchfork bifurcation occurring at the parameter point $\alpha = \alpha_p \approx 4.6691$ which belongs to the curve N_p shown in Fig. 5(a). Before the bifurcation (for $\alpha < \alpha_p$), the fixed point $x^{(1)}$ is stable (shown with a red line), after the bifurcation (for $\alpha > \alpha_p$) it is unstable (shown with a blue line), and two stable fixed points $x^{(2)}, x^{(3)}$ have appeared. (b) Multiplier diagram. At the point $\alpha = \alpha_p$, the multiplier ρ of the fixed point $x^{(1)}$ crosses through $+1$. $\Gamma = 43$.

Examples for the case (b) mentioned above are shown in Fig. 8. As one can see in Fig. 8(a), the bifurcations occurring at $\alpha_1 \approx 4.6586033$ and $\alpha_4 \approx 4.6586209$ are supercritical border-collision period-doubling bifurcations. Note that the stable 2-cycle existing between these bifurcations undergoes two further border collisions (at $\alpha_2 \approx 4.6586120$ and $\alpha_3 \approx 4.6586122$) of the persistence type. A similar example for a border-collision period-doubling bifurcation is shown in Fig. 8(b), at $\alpha_5 \approx 4.658797$.

It is remarkable in Fig. 8(a) that for increasing values of α we observe first the appearance and then the disappearance of a stable 2-cycle. After a momentary destabilization, the fixed point is stable again and eventually, for further increasing values of α it will be destabilized and restabilized again and again, before the final transition to chaos occurs. This leads to the complexity of the boundary between the domain of stable fixed points $\Pi_1 \cup \Pi_{1,1}$ and the chaotic domain Π_∞ shown in Fig. 5.

The mechanism leading to destabilization and eventually restabilization of a fixed point is illustrated in Fig. 9. Let us consider the four branches of the function f^m , denoted for the sake of clarity by f_1^m, \dots, f_4^m , as shown in Fig. 9. Let s_{ij} denote the border point of f^m at which the branches f_i^m and f_j^m (with $i, j \in 1, \dots, 4$) are adjacent. To explain the observed phenomenon, we note that when α increases in the considered range, then the branches f_1^m and f_4^m move upwards and the border points s_{12} and s_{34} move towards each other.

Before the first border-collision period-doubling bifurcation (at $\alpha \approx 4.658602 < \alpha_1$, see Fig. 9(a)), the fixed point belongs to the stable branch²¹ f_2^m . At the bifurcation moment, i.e., for $\alpha = \alpha_1 \approx 4.6586033$, it collides with the border point

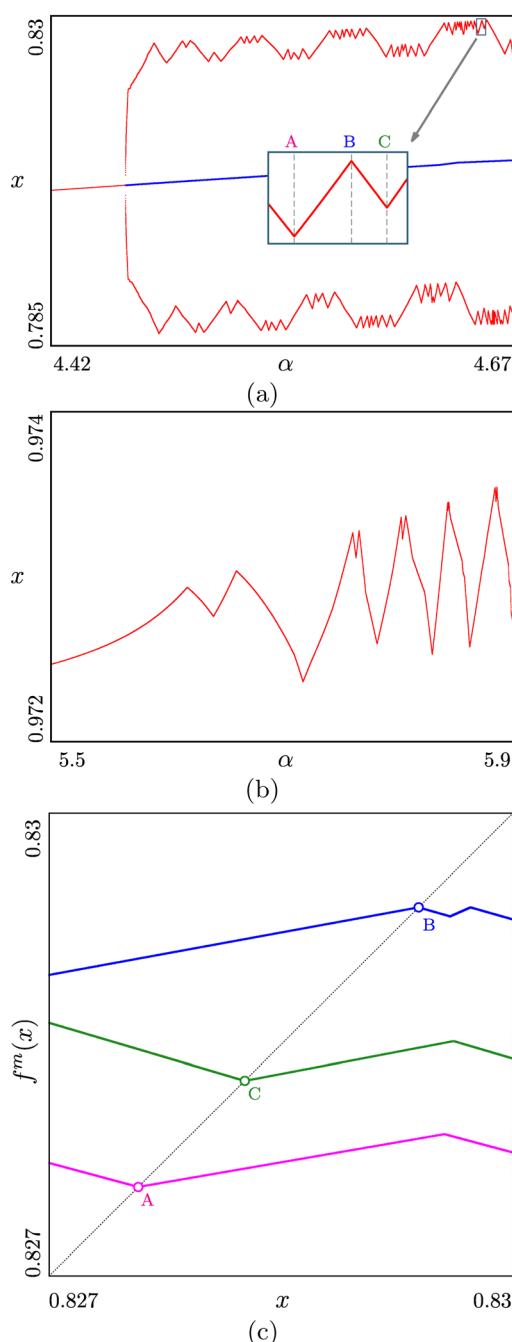


FIG. 7. Cascades of border collisions of stable fixed points (a) after a pitchfork bifurcation (at $\Gamma = 45$) and (b) in the absence a pitchfork bifurcation (at $\Gamma = 36$). As in Fig. 6, stable fixed points are shown with red lines and unstable ones with blue lines. Inset in (a) shows the marked rectangle enlarged. The stable fixed points at the moment of border collisions at $\alpha \approx 4.650934$, $\alpha \approx 4.652986$, and $\alpha \approx 4.654263$ marked in the inset with A, B, and C, respectively, are shown in (c).

s_{12} . Immediately after the border-collision period-doubling bifurcation, the fixed point belongs to the unstable branch f_1^m , and the points of the stable 2-cycle are located on the branches f_1^m and f_2^m (see Fig. 9(b)), which corresponds to $\alpha_1 < \alpha \approx 4.658606 < \alpha_2$). In this way, as a result of a border-collision period-doubling bifurcation, an absorbing interval $J = [f^m(s_{12}), f^{2m}(s_{12})]$ appears.

For increasing values of α , the border point s_{23} and eventually also the border point s_{34} enter the absorbing interval

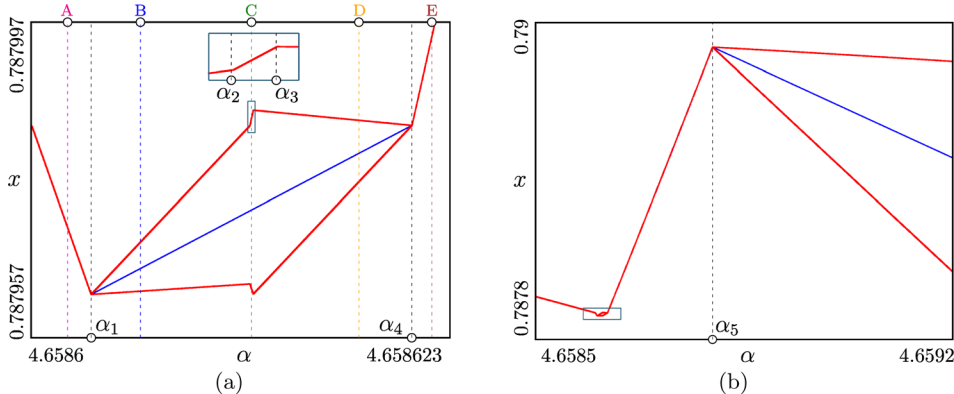


FIG. 8. Appearance and disappearance of a 2-cycle via supercritical border-collision period-doubling bifurcations. Inset in (a) shows the marked rectangle enlarged; two border collisions of the 2-cycle are clearly visible. The rectangle marked in (b) corresponds to (a). $\Gamma = 45$.

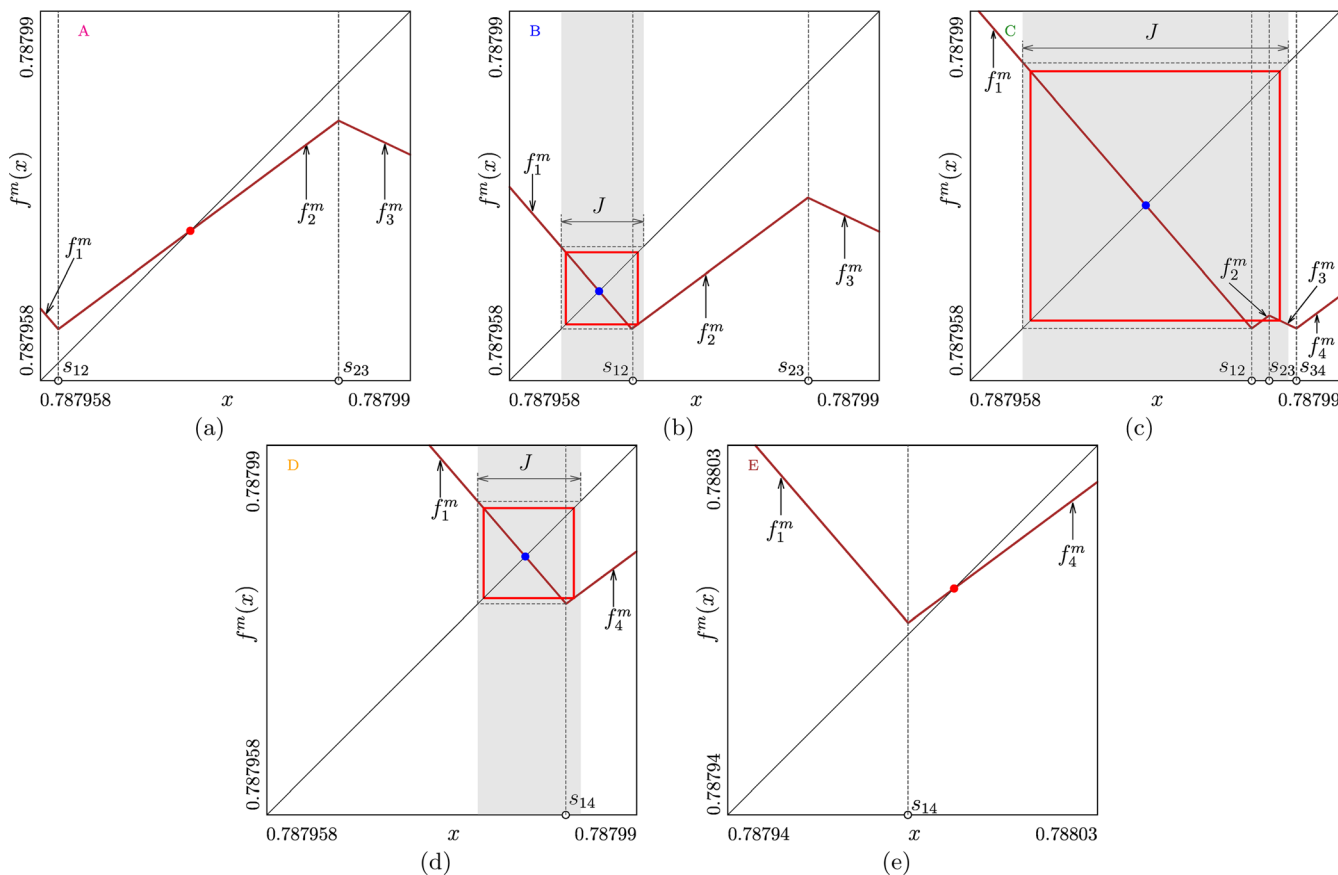


FIG. 9. Shapes of the relevant part of the function f^m are shown at $\alpha \approx 4.65093$, $\alpha \approx 4.65299$, $\alpha \approx 4.65426$, $\alpha \approx 4.65299$, and $\alpha \approx 4.65299$ marked in Fig. 8(a) with A, B, C, D, and E, respectively. In (b)–(d), the invariant absorbing interval J is shown. $\Gamma = 45$.

J . The corresponding parameter values are given by the conditions $f^{2m}(s_{12}) = s_{23}$ and $f^{2m}(s_{12}) = s_{34}$, respectively. However, this has no direct influence on the asymptotic dynamics until at $\alpha = \alpha_2 \approx 4.658612009$ the 2-cycle undergoes a border collision, as its right point collides with the border point s_{23} . So, between $\alpha = \alpha_2$ and $\alpha = \alpha_3$ the right point of the cycle belongs to the stable branch f_3^m (see Fig. 9(c), which corresponds to $\alpha_2 < \alpha \approx 4.6586121 < \alpha_3$), and the cycle remains stable. At $\alpha = \alpha_3 \approx 4.658612204$, the 2-cycle undergoes the next border collision, caused by the collision of its right point with s_{34} . Thereafter, the right point of the cycle belongs to the stable branch f_4^m which, for increasing α , moves upwards, causing the 2-cycle to shrink. Moreover, at some value of α between α_3 and α_4 the branches f_2^m and f_3^m

disappear, as the border points s_{12} , s_{23} , and s_{34} merge into a single border point s_{14} . After this collision only the branches f_1^m and f_4^m , at which the stable 2-cycle is located, remain. Accordingly, the absorbing interval is now given by $J = [f^m(s_{14}), f^{2m}(s_{14})]$. For further increasing α , the absorbing interval J and the 2-cycle continue to shrink (see Fig. 9(d), which corresponds to $\alpha_3 < \alpha \approx 4.658618 < \alpha_4$). Then, at the second border-collision period-doubling bifurcation (at $\alpha = \alpha_1 \approx 4.6586209$) the cycle disappears and the fixed point moves to the branch f_4^m which is necessarily stable (see Fig. 9(e)).

With some variation, the mechanism described above is repeated several times. For example, the sequence of bifurcations shown in Fig. 8(b) starts with a border-collision period-

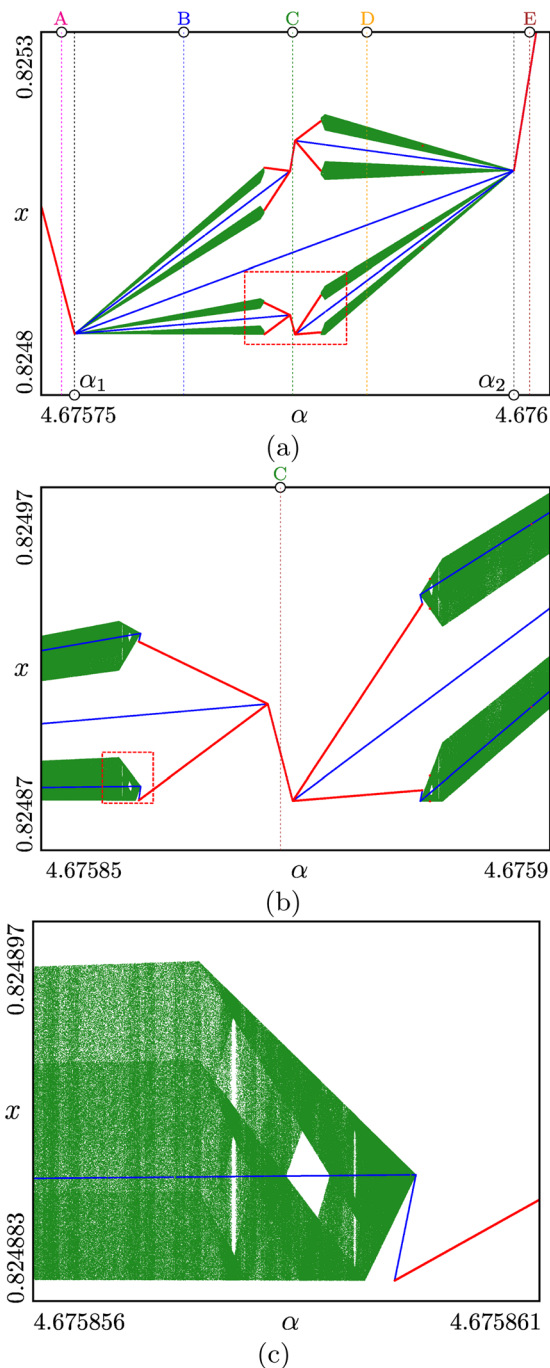


FIG. 10. Appearance and disappearance of a 4-band chaotic attractor. Rectangles outlined in (a) and (b) are shown magnified in (b) and (c), respectively. $\Gamma = 45$.

doubling bifurcation at $\alpha = \alpha_5$ and follows the same pattern. In this case, the disappearance of the 2-cycle is related not to a border-collision period-doubling bifurcation but to a border-collision fold bifurcation, as described below. However, the overall effect is the same, as eventually the fixed point moves to a stable branch of f_m and thus is stabilized again.

The mechanism described above is not necessarily associated with the appearance of a 2-cycle. In fact, for increasing or decreasing values of α the same mechanism may lead to the appearance and disappearance of n -band chaotic

attractors with $n = 2^\ell$, $\ell = 0, 1, 2, \dots$ (case (c) mentioned above). An example of that is shown in Fig. 10(a). The border-collision bifurcations occurring at $\alpha_1 \approx 4.6757663$ and $\alpha_2 \approx 4.6759822$ lead from a stable fixed point to a 4-band chaotic attractor as well as to an unstable fixed point and an unstable 2-cycle.

As in the previous example, the destabilization and restabilization of a fixed point are associated with the disappearance of two branches of map (7). Numbering the branches of the map as in the previous example, and considering the location of the attractors for increasing values of α , we find that, immediately before α_1 , a stable fixed point is located on the branch f_2^m (see Fig. 11(a)). After the border-collision bifurcation that occurs when this fixed point collides with the border point s_{12} , the map has an invariant absorbing interval $J = [f^m(s_{12}), f^{2m}(s_{12})]$, and once the orbit has entered this interval, the complete asymptotic dynamics takes place inside it. As in the previous example, inside this interval there is an unstable fixed point on the branch f_1^m , surrounded by a 2-cycle whose points belong to the branches f_1^m and f_2^m . The difference to the previous example is associated with the fact that the absolute value of the slope of the branch f_1^m is higher. As a consequence, a 2-cycle appearing after the bifurcation is unstable and the map has a 4-band chaotic attractor located on the branches f_1^m and f_2^m (see Fig. 11(b)). Note that as long as $f^{2m}(s_{12}) < s_{23}$, the point s_{12} is the only border points inside J . Therefore, the boundaries of the chaotic attractor are completely determined by the images of s_{12} and are given by $f^{j-m}(s_{12})$ with $j = 1, \dots, 8$.

For increasing values of α , the border points s_{12} and s_{23} move closer to each other so that at $\alpha \approx 4.6758577$ the border point s_{23} enters the interval J (as in the previous example, the value of α when it occurs is determined by the condition $f^{2m}(s_{12}) = s_{23}$). When the point s_{23} is located inside J , its images determine the boundaries of the chaotic attractor, which are now given by $f^{j-m}(s_{23})$ with $j = 1, \dots, 8$. Moreover, as the dynamics of a map with two border points in the absorbing interval can be significantly more complicated than the dynamics of a map with one such point, several multi-band chaotic attractors appear (see Fig. 10(c)). In any case, the border collisions occurring at the points s_{12} and s_{23} lead to the appearance of a stable 4-cycle (see Fig. 11(c)). This may be associated with a direct transition from a 4-band chaotic attractor to a stable 4-cycle, or, as illustrated in Fig. 10(b), with border-collision fold bifurcation of a 4-cycle which leads to the coexistence of a chaotic attractor and a stable 4-cycle. Eventually, once the branches f_2^m and f_3^m have disappeared, a 4-band chaotic attractor located on the branches f_1^m and f_4^m exists (see Fig. 11(d)), until the border-collision bifurcation occurring at $\alpha = \alpha_2$, where a stable fixed point appears at the branch f_4^m (Fig. 11(e)).

In fact, sequences of bifurcations between destabilization and restabilization of a fixed point may be even more complicated than illustrated in Figs. 8 and 10. An example hereof is shown in Fig. 12. As one can see, the 4-band chaotic attractor which appears at the border-collision bifurcation at $\alpha_1 \approx 4.676082$ disappears again at a border-collision fold bifurcation (at $\alpha_4 \approx 4.6766085$) at which also two unstable 2-cycles disappear. Similarly, the 2-band chaotic

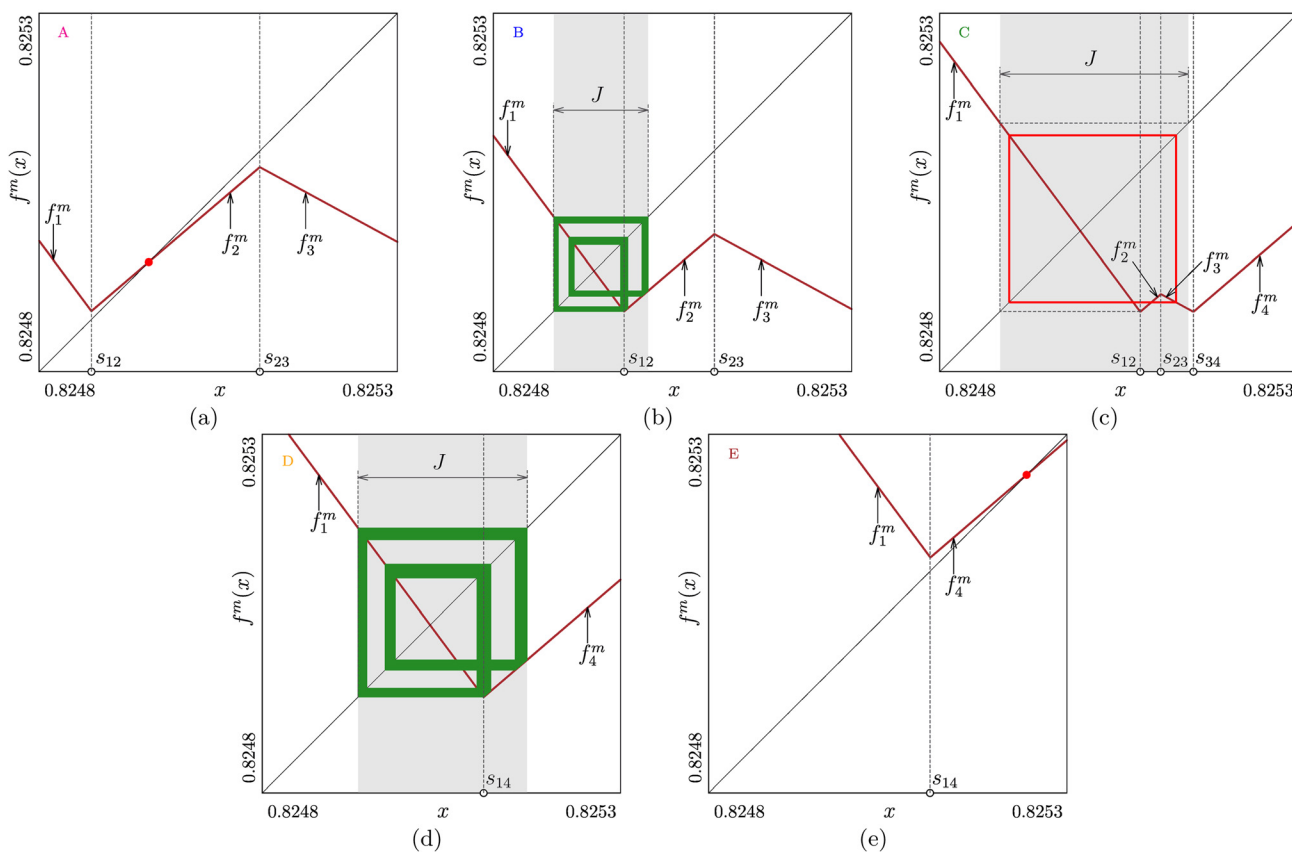


FIG. 11. Relevant branches of f^m are shown at $\alpha \approx 4.67576$, $\alpha \approx 4.67582$, $\alpha \approx 4.6758735$, $\alpha \approx 4.67591$, and $\alpha \approx 4.67599$ marked in Fig. 10(a) with A, B, C, D, and E, respectively. In (b)–(d), the invariant absorbing interval J is shown. $\Gamma = 45$.

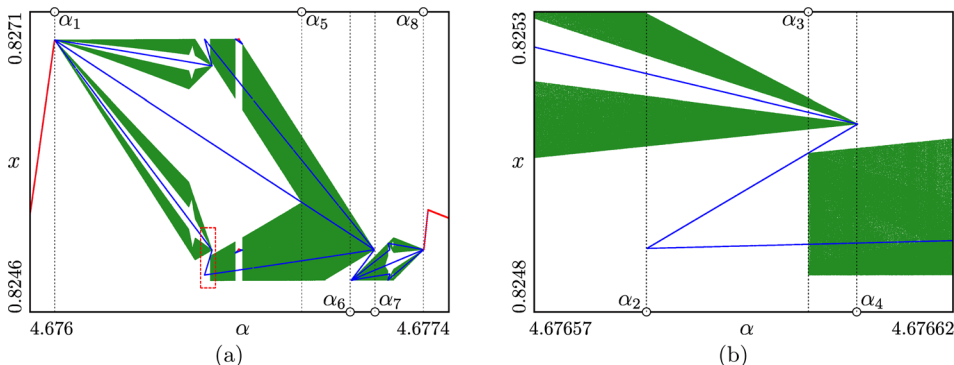


FIG. 12. Appearance and disappearance of several (one-, two-, and four-band) chaotic attractors. Coexistence of chaotic attractors is clearly visible in the parameter intervals (α_3, α_4) and (α_6, α_7) . In (b), the red rectangle outlined in (a) is shown magnified. $\Gamma = 45$.

attractor which appears at the border-collision bifurcation at $\alpha_8 \approx 4.677315$ for decreasing α turns into a one-band chaotic attractor and eventually disappears in a border-collision fold bifurcation (at $\alpha_6 \approx 4.67707$) related to the disappearance of two unstable fixed points. Moreover, at $\alpha_7 \approx 4.677153$ a different one-band chaotic attractor appears also at a border-collision fold bifurcation, at which (for decreasing α) two unstable fixed points appear. As $\alpha_6 < \alpha_7$, chaotic attractors coexist in the interval (α_6, α_7) . With further decreasing values of α this attractor is split into two bands (a band-merging bifurcation occurring at $\alpha = \alpha_5 \approx 4.676908$), to be interrupted by a small periodicity window of a stable 2-cycle, and finally to disappear at $\alpha = \alpha_3 \approx 4.676603$.²² By contrast to other bifurcations leading to disappearance of chaotic attractors,

the bifurcation occurring at $\alpha = \alpha_2$ is a final bifurcation (boundary crisis), caused by the collision of the attractor with an unstable 2-cycle. Note that as $\alpha_2 < \alpha_3$, a two-band and a 4-band chaotic attractor coexist in the parameter interval (α_2, α_3) . For even smaller values of α , immediately after the final bifurcation the typical orbit converges to the 4-band chaotic attractors, but there exists still a chaotic repeller, which disappears at $\alpha = \alpha_2 \approx 4.6765875$ in a border-collision fold bifurcation related to two unstable 2-cycles.

For a fixed Γ , blocks similar to the bifurcation sequences described above appear more and more frequently for increasing α . As a result, the stability intervals of fixed points become smaller and smaller until they disappear completely. This leads to the complex structure of the region in the

parameter space close to the boundary between the stability domain of fixed points $\Pi_1 \cup \Pi_{1,1}$ and the chaotic domain Π_∞ (see Fig. 5).

IV. CONCLUSION

The normal operational regime for the considered class of converter systems is the regime of stable period-1 dynamics. Different types of feedback correctors may be used in order to obtain a faster response, a more accurate control, or a higher efficiency. However, in practice it is not easy to adjust the parameters, such that an operating mode with the desired dynamic characteristics is obtained. When parameters are varied, the period-1 operating mode may lose stability. This is known to lead to the appearance of complex dynamics, including subharmonic and chaotic oscillations.^{4,12}

In general, complex dynamics in power electronic DC/AC converters is caused by the presence of two externally applied oscillatory modes (the ramp cycle and the reference signal). The appearance of significant fluctuations associated with the rapid switching dynamics has been observed in practical inverter systems,¹ and has been confirmed by experiments in the present work. However, this phenomenon and the associated unusual transition to chaos appear not previously have been explained in detail. In the present work, we considered a model of a single-phase H-bridge inverter with pulse-width modulated control. The behavior of this inverter was described by a non-autonomous piecewise-smooth map $F(x_k, k)$ given by Eq. (4). Note that the stable period-1 dynamics with the period $\bar{T} = m$ of the continuous-time system (3) (which corresponds to the normal operational regime of the converter considered in this paper) is represented in the one-dimensional autonomous stroboscopic map (7) by a stable fixed point. With respect to the properties of this stroboscopic map it is worth noticing that it corresponds to the m th iterate of the map $F(x_k, k)$. To ensure a good quality of the output signal, i.e., to decrease the amplitude of undesired distortion of the wave form, it is necessary to use a sufficiently large value of m . Accordingly, the number of border points of f^m may become very high, as it grows exponentially with increasing m . This leads to a complex shape of the boundary between the region in the parameter space corresponding to stable fixed points of the stroboscopic map (or, in other words, to the desired mode of operation of the considered inverter) and the chaotic domain. It is well known that piecewise-smooth maps with a single border point may show a direct transition from a stable fixed point to chaos via a single border-collision bifurcation. Clearly, such bifurcations occur in our map (7). However, the transition from the parameter region corresponding to the normal operational regime of the inverter to the chaotic domain is essentially related to the existence of a high number of border points of f^m . Possibly (but not necessarily) after an initial pitchfork bifurcation, we observe a sequence of border collisions. At the beginning, these border collisions are associated with transitions of a fixed point from one stable branch to another one. This leads to persistence of a stable fixed point after such a border collision. It is worth to note that a

high number of such border collisions are not only due to a high number of branches of f^m but also to the non-monotonous dependence of the amplitude of f^m on the corrector gain factor α . As α increases, the value $f^m(x)$ for any particular x may either increase or decrease.

For increasing values of some of the branches of f^m become unstable. Then the fixed point after the border collision is unstable, an absorbing interval J appears, and the attractor of f^m located inside this interval may be either a stable 2^k -cycle, $k \geq 1$, or a 2^k -band chaotic attractor, $k \geq 0$. At the beginning, there are only a few unstable branches of f^m , so that we observe a destabilization and eventually restabilization of fixed points. Particular sequences of border-collision bifurcations are caused predominantly caused by the entrance of new branches of f^m in the absorbing interval J and by disappearance of previously existing branches of f^m inside the absorbing interval J . For increasing values of α , more and more branches of f^m become unstable, so that stability intervals of fixed points become smaller. Eventually, all branches of f^m are unstable so that only chaotic dynamics remains.

Further development of the investigations discussed in the present work is important both from the theoretical and applied points of view, as it will provide a theoretical foundation for design and control of a wide class of DC/AC power converter systems and similar applications. At the present stage, many questions are still open, as, for example, the behavior of the boundary described in the present work in the limiting case $m \rightarrow \infty$. Preliminary works show that it is promising to apply concepts of symbolic dynamics to map (4), as well as the mapping dynamics technique,²³ since the Poincaré mapping from the switching manifold Σ to itself can be obtained for system (3) analytically.

ACKNOWLEDGMENTS

V. Shein and E. Khrantsov are acknowledged for their help in implementing the experimental setup. V. Avrutin was supported by the European Community within the scope of the project “Multiple-discontinuity induced bifurcations in theory and applications” (Marie Curie Action of the 7th Framework Programme), and by the German Research Foundation within the scope of the project “Organizing centers in discontinuous dynamical systems: Bifurcations of higher codimension in theory and applications.”

¹M. Kazmierkowski, R. Krishnan, and F. Blaabjerg, *Control in Power Electronics—Selected Problems* (Elsevier Science, 2002).

²W. Weimin, H. Yuanbin, and F. Blaabjerg, *IEEE Trans. Power Electron.* **27**, 782 (2012).

³Siemens press release “Estlink 2: 650 kW, 450 kV DC transmission between Finland and Estonia” (December 23, 2010).

⁴Zh. T. Zhusubaliyev, E. Mosekilde, A. I. Andriyanov, and V. V. Shein, *Physica D* **268**, 14 (2014).

⁵V. Anishchenko, S. Nikolaev, and J. Kurths, *Phys. Rev. E* **73**, 056202 (2006).

⁶J. L. Laugesen, E. Mosekilde, and N.-H. Holstein-Rathlou, *Chaos* **21**, 033128 (2011).

⁷*Nonlinear Phenomena in Power Electronics*, edited by S. Banerjee and G. C. Verghese (IEEE Press, New York, USA, 2001).

- ⁸Zh. T. Zhusubaliyev and E. Mosekilde, *Bifurcations and Chaos in Piecewise-Smooth Dynamical Systems* (World Scientific, Singapore, 2003).
- ⁹M. di Bernardo, C. J. Budd, A. R. Champneys, and P. Kowalczyk, *Piecewise-Smooth Dynamical Systems: Theory and Applications* (Springer-Verlag, London, 2008).
- ¹⁰M. di Bernardo, A. Nordmark, and G. Olivar, *Physica D* **237**, 119 (2008).
- ¹¹O. Makarenkov and J. Lamb, *Physica D* **241**, 1826 (2012).
- ¹²Zh. T. Zhusubaliyev, E. Mosekilde, A. I. Andriyanov, and G. Y. Mikhail'chenko, *Electronics* **2**, 113 (2013).
- ¹³A. Luo, *Int. J. Bifurcation Chaos* **24**, 1430013 (2014).
- ¹⁴C. Hsu, *Cell-to-Cell Mapping: A Method of Global Analysis for Nonlinear Systems*, Applied Mathematical Sciences Vol. 64 (Springer, 1987).
- ¹⁵G. Osipenko, *Dynamical Systems, Graphs, and Algorithms*, Lecture Notes in Mathematics Vol. 1889 (Springer, 2007).
- ¹⁶V. Avrutin, P. Levi, M. Schanz, D. Funderinger, and G. Osipenko, *Int. J. Bifurcation Chaos* **16**, 3451 (2006).
- ¹⁷S. Ito, S. Tanaka, and H. Nakada, *Tokyo J. Math.* **2**, 241 (1979).
- ¹⁸F. Takens, in *Dynamical Systems and Bifurcation Theory*, Pitman Research Notes in Mathematics Series Vol. 160, edited by M. Camacho, M. Pacifico, and F. Takens (Longman Scientific and Technical, 1987), pp. 399–421.
- ¹⁹Yu. L. Maistrenko, V. L. Maistrenko, and L. O. Chua, *Int. J. Bifurcation Chaos* **3**, 1557 (1993).
- ²⁰I. Sushko and L. Gardini, *Int. J. Bifurcation Chaos* **20**, 2045 (2010).
- ²¹Rigorously speaking, the terms “stable” or “unstable” cannot be applied to branches of f^m without further explanation, as these branches are given by nonlinear functions. Still, for simplicity we use these terms, as for the considered parameter values the branches of f^m are almost linear. We call a branch stable if it is everywhere contractive, unstable if it is everywhere expanding, and neglect the case related to the presence of contractive and expanding parts within the same branch of f^m .
- ²²For an overview regarding bifurcation of chaotic attractors in 1D maps and in particular for conditions of their occurrence, we refer to the recent paper V. Avrutin, L. Gardini, M. Schanz, and I. Sushko, *Int. J. Bifurcation Chaos* **24**, 1440012 (2014).
- ²³A. Luo, *J. Sound Vib.* **283**, 723 (2005).